Journal of Superconductivity: Incorporating Novel Magnetism, Vol. 17, No. 1, February 2004 (© 2004)

Atomic Scale Elastic Textures Coupled to Electrons in Superconductors

K. H. Ahn,[1] Jian-Xin Zhu,[1] Z. Nussinov,[1] T. Lookman,[1] A. Saxena,[1] A. V. Balatsky,[1] and A. R. Bishop[1]

Received 10 August 2003

We present an atomic scale theory of lattice distortions using strain-related variables and their constraint equations. Our approach connects constrained *atomic length* scale variations to *continuum* elasticity and can describe elasticity at all length scales. We apply the general approach to a two-dimensional square lattice with a monatomic basis, and find the atomic scale elastic textures around a structural domain wall and a single defect, as exemplar textures. We clarify the microscopic origin of anisotropic gradient terms, some of which are included phenomenologically in Landau–Ginzburg theory. The obtained elastic textures are used to investigate the effects of elasticity-driven lattice deformation on the nanoscale electronic structure in superconductor by solving the Bogliubov–de Gennes equations with the electronic degrees of freedom coupled to the lattice ones. It is shown that the order parameter is depressed in the regions where the lattice deformation takes place. The calculated local density of states suggests the electronic structure is strongly modulated as a response to the lattice deformation—the elasticity propagates the electronic response over long distances. In particular, the trapping of low-lying quasiparticle states around the defects is possible. These predictions could be directly tested by STM experiments in superconducting materials.

KEY WORDS: elasticity textures; nanoscale electronic structure; superconductors.

In many complex electronic materials such as cuprates, manganites, ferroelastic martensites, and titanates, unexpected multiscale modulations of charge, spin, polarization, and strain variables have been revealed by high-resolution microscopy [1]. It is increasingly evident that the nonuniform textures found in these doped materials have intrinsic origins: they arise from coupling between various degrees of freedom. The textures fundamentally affect local and mesoscopic electronic, magnetic, and structural properties, which are central to the functionality of correlated electronic materials. There is substantial evidence for significant coupling amongst the electronic degrees of freedom with the lattice distortions in cuprates, manganites, and ferroelectrics. The charge carrier doping can act as a local stress to deform surrounding unit cells [1]. We might employ a Landau–Ginzburg (LG) theory to study the coupling between the electronic (Cooper pair) and lattice (strain tensor) degrees of freedom in superconductors. However, the LG theory can only rigorously describe the long wavelength behavior. New generations of experimental tools to probe individual atoms and local environments [2], and the aforementioned growing interest in complex functional materials, emphasize the importance of accurately describing the local electronic properties and lattice distortion at the atomic scale. In this work, we first present a microscopic description of elasticity. We introduce appropriate *inter*- and *intra*-cell distortion modes and show how the form of the elastic energy recovers the correct phonon spectra. The discreteness of the lattice, choice of modes and constraints among them give rise to an anisotropic gradient expansion for the elastic energy. This leads to interesting elastic domain wall and defect textures. We then couple these textures to the electronic degrees of freedom and study microscopically the influence of strain

[1]Theoretical Division, Los Alamos National Laboratory, Los Alamos, New Mexico 87545.

0896-1107/04/0200-0007/0 © 2004 Plenum Publishing Corporation

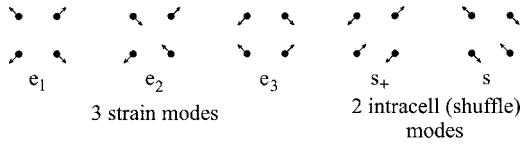

Fig. 1. Normal distortion modes for a square object of four atoms in 2D.

on electronic wavefunctions in both s- and d-wave superconductors.

Our approach is general, but we illustrate it here in detail for the simplest case, namely a square lattice in two-dimensional (2D) space with a monatomic basis. We find that the most convenient strain-related variables for atomic scale distortions are the normal distortion modes of an elementary square object of four atoms (Fig. 1). The first three distortion modes in Fig. 1 correspond to the usual dilatation (e_1), shear (e_2), and deviatoric (e_3) strains of the continuum elasticity theory for a square lattice [3]. The next two degenerate modes in Fig. 1, s_+ and s_-, correspond to the "intracell" or "shuffle" modes of the square lattice [4], which are absent in continuum elasticity theory. Our approach uses these five distortion variables defined for each plaquette of four atoms at $\vec{i}, \vec{i}+(10), \vec{i}+(11)$, and $\vec{i}+(01)$, where $\vec{i}$ represents the coordinate of the lattice points, to describe the elastic energy [5].

Since the five variables are derived from two displacement variables for each lattice site, they are related by three constraint equations. By representing e_1, e_2, e_3, s_+, and s_- in terms of displacement variables d^x and d^y in k (wave vector) space and eliminating d^x and d^y, the constraint equations are obtained. One of them is the *microscopic* elastic compatibility equation, which relates strain modes:

$$(1-\cos k_x\,\cos k_y)e_1(\vec{k}) - \sin k_x\,\sin k_y e_2(\vec{k}) + \cos k_x - \cos k_y)e_3(\vec{k}) = 0. \quad (1)$$

The other two relate the intracell and the strain modes:

$$2\cos\frac{k_x}{2}\,\cos\frac{k_x}{2}s_\pm(\vec{k}) \mp i\sin\left(\frac{k_x \pm k_y}{2}\right)e_1(\vec{k}) \pm i\sin\left(\frac{k_x \mp k_y}{2}\right)e_3(\vec{k}) = 0. \quad (2)$$

These constraints generate *anisotropic* interactions (from the lattice symmetry) between atomic scale strain fields, similar to the compatibility equations in continuum theory [3], but now including the intracell modes. In the long wavelength limit, our description naturally reproduces the continuum results: For $\vec{k} \to 0$, the above constraint equations can be written in real space as

$$\nabla^2 e_1(\vec{r}) - 2\nabla_x\nabla_y e_2(\vec{r}) + \left(\nabla_y^2 - \nabla_x^2\right)e_3(\vec{r}) = 0, \quad (3)$$

$$s_\pm(\vec{r}) = \frac{1}{4}[(\nabla_y \pm \nabla_x)e_1(\vec{r}) + (\nabla_y \mp \nabla_x)e_3(\vec{r})]. \quad (4)$$

Equation (3) is the familiar compatibility equation in continuum theory. Equation (4) shows that *the spatial variations of strains always generate intracell modes*, the magnitudes of which vanish as the inverse of the length scale of the strain mode variations. In continuum LG theory, the energy associated with the gradient of strains is responsible for domain wall energies as, e.g., in structural phase transitions [4]. The above result shows that the intracell modes are the origin of such energy terms. Since our strain-related variables become identical to conventional strain variables for $k \to 0$, various length scale lattice distortions may be described in a *single* theoretical framework. This makes it possible to study typical multiscale situations where both short- and long-wavelength distortions are important (and coupled). It also provides a natural framework for incorporating interactions between atomic scale strain-related fields coupled to other degrees of freedom in functional materials (below).

The following analysis of the simple harmonic elastic energy for the square lattice further exemplifies the utility of these variables. We consider the simplest energy expression by approximating the total elastic energy as the sum of the elastic energy of each square:

$$E_{\text{sq,lat}} = \sum_{\vec{i}} \left\{ \sum_{n=1,2,3} \frac{1}{2} A_n [e_n(\vec{i})]^2 + \sum_{m=+,-} \frac{1}{2} B[S_m(\vec{i})]^2 \right\}, \quad (5)$$

where A_n and B denote elastic moduli and "intracell modulus," respectively. Since some of the atomic pairs are shared by two square plaquettes of atoms, the parameters in Eq. (5) should be appropriately renormalized. A robust way to determine the parameters is to compare the phonon spectrum of our model with experimental data.

The phonon spectrum has been obtained [6]. A typical spectrum (upper branch) for $A_1 = 5$, $A_2 = 4$, $A_3 = 3$, and $B = 5$ is shown in Fig. 2a. At $\vec{k} = (\pi, \pi)$, the distortion is a pure intracell mode, and the energy depends only on the intracell mode modulus B. Therefore, as shown in Fig. 2b, $\omega(\pi, \pi)$ vanishes without including the intracell mode ($B = 0$), which is unphysical.

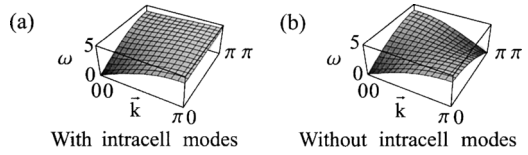

Fig. 2. An example of calculated phonon spectra (a) with and (b) without intracell modes for a 2D square lattice with a monatomic basis. The upper phonon branch is shown for both cases ($M = \hbar = 1$).

We apply our formalism to obtain the domain wall solution for the atomic displacements between two homogeneous strain states (a "twin boundary") due to a phase transition to a rectangular lattice. We then compare the solution to that obtained from continuum theory, where discreteness effects are neglected [4]. With elastic energy $E_{\rm rec} = E^{(1)}_{\rm rec} + E^{(2)}_{\rm rec}$,

$$E^{(1)}_{\rm rec} = \sum_{\vec{i}} \frac{1}{2} A_1 e_1(\vec{i})^2 + \frac{1}{2} A_2 e_2(\vec{i})^2 + \frac{1}{2} B[s_+(\vec{i})^2 + s_-(\vec{i})^2],$$

$$E^{(2)}_{\rm rec} = \sum_{\vec{i}} -\frac{1}{2} A_3' e_3(\vec{i})^2 + \frac{1}{4} F_3 e_3(\vec{i})^4, \qquad (6)$$

the degenerate ground state of $E_{\rm rec}$ is a uniform state with $e_3 = \pm\sqrt{A_3'/F_3}$, and $e_1 = e_2 = s_+ = s_- = 0$. To study the domain wall between these two degenerate rectangular ground states, we consider $e_3(\vec{i})$ as the order parameter and minimize $E^{(1)}_{\rm rec}$ with respect to the other variables, using the constraint equations (Eqs. (1) and (2)) and the method of Lagrange multipliers. We obtain $E^{(1)}_{\rm rec,min} = \sum_{\vec{k}} \frac{1}{2} e_3(-\vec{k}) U(\vec{k}) e_3(\vec{k})$, where $U(\vec{k})$ is given in Ref. [6].

With $k_x = k\cos\theta$ and $k_y = k\sin\theta$, the expansion of $U(k,\theta)$ about $k = 0$ yields $U(k,\theta) = U_0(\theta) + U_2(\theta)k^2 + O(k^4)$, where $U_0(\theta) = A_1 A_2 \cos^2 2\theta / (A_1 \sin^2 2\theta + A_2)$, and $U_2(\theta) = \sin^2 2\theta[6A_1A_2B \sin^2 2\theta + 4A_1A_2(A_1 + A_2) \cos^2 2\theta + 3B(A_2^2 + A_1^2 \sin^2 2\theta)]/[24(A_2 + A_1 \sin^2 2\theta)^2]$. The term U_0-is purely orientation-dependent without a length scale, and is minimized at $\theta = 45$ and 135° as obtained in Ref. [3]. The difference between continuum and our discrete theories lies in the k^2 term: continuum theory commonly assumes isotropic gradients in the order parameter, i.e., $(\vec{\nabla} e_3)^2$ [4], whereas $U_2(\theta)$ is anisotropic. The two origins of the anisotropy are (a) the compatibility relation, Eq. (1), which has higher powers in k than Eq. (3) because of discreteness, and (b) the presence of the shuffle mode energy. The latter can be written as gradients of strains, but with corrections to the phenomenological isotropic term, $(\vec{\nabla} e_3)^2$, commonly used in LG theory. As $U_2(\theta)$ is minimized for $\theta = 0$ and 90°, it competes with $U_0(\theta)$ which prefers $\theta = 45$ and 135°. Thus, the domain wall direction depends on the length scale with a critical length scale $\lambda_c \sim \sqrt{B/A_1}$. If $\lambda_c \leq 1$, i.e., less than the interatomic spacing, the domain wall has direction 45 or 135° down to atomic scales. If $\lambda_c > 1$, then for length scales smaller (larger) than λ_c, the domain wall direction is 0 or 90° (45 or 135°) and the domain wall has multiscale attributes.

We examine first the case $\lambda_c \leq 1$ that would apply to materials with relatively large bulk modulus A_1 ('hard' materials) for fixed B. Here $k_x = \pm k_y$ and $U(\vec{k}) = B(1 - \cos k_x)/(1 + \cos k_x)$. In Fig. 3, we illustrate the domain wall solution with 135° domain wall direction.The only nonzero distortion modes are e_3 and s_- (s_+ for a 45° domain wall). The strain e_3 reverses sign at the domain wall, the intracell mode s_- is confined within the domain wall, and the atomic displacements are parallel to the domain wall direction. The numerical solution for e_3 and s_- along a line perpendicular to the wall is shown in Fig. 3a, for which $\lambda_c \sim 1$. The e_3 field and the corresponding displacement field near the center of the domain wall are shown in Figs. 4a and b, in which grayscales show regions with e_3 positive and negative, respectively. Both figures show that the center of the domain wall is located at bonds rather than sites to avoid the higher energy state of $e_3 = 0$ and large s_-. In Fig. 3b we compare our results with continuum theory, which predicts $e_3 = e_3^{\max} \tanh(i_s/\xi)$ [4] and $s_- = \partial e_3/2\partial i_s$ from

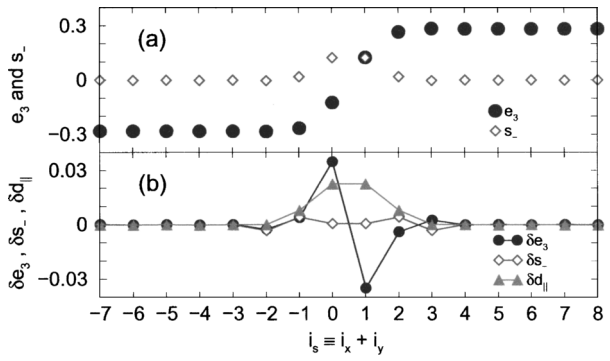

Fig. 3. Atomic scale 135° domain wall profile for critical length scale, $\lambda_c \leq 1$ along the direction perpendicular to the domain wall: (a) strain e_3 and shuffle s_-; (b) differences in e_3 ($\delta e_3 = e_{3,\rm atomic} - e_{3,\rm continuum}$), s_- (δs_-) and displacement parallel to the domain wall direction ($d_\parallel$) between the results from continuum theory for $\bar{k} \sim 0$ and our model that includes discreteness. Parameter values are $A_1 = 5$, $A_2 = 4$, $A_3' = 4$, $B = 5$, and $F_3 = 50$.

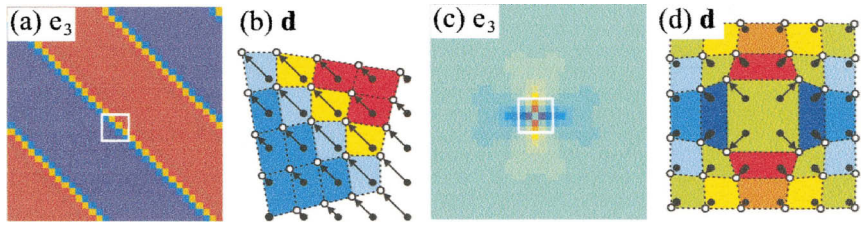

Fig. 4. Strain-e_3 mode for a periodic twinned microstructure (a) and a single defect (c) together with their corresponding displacement configurations ((b) and (d)) within the highlighted window. $N_L = 32 \times 32$.

Eq. (4), where $i_s = i_x + i_y$. The differences in the interface region, shown in Fig. 3b, are of the order of 10% of $e_3^{\max} = \sqrt{A_3'/F_3}$.

The domain wall solution for $\lambda_c > 1$, typical for small bulk modulus A_1 ('soft' materials) is shown in Fig. 5 for which $\lambda_c \sim \sqrt{5}$. The e_3 field in Fig. 5a shows that on length scales of the size of the system (larger than λ_c), the diagonal orientation is still preferred. However, this diagonal domain wall consists of a 'staircase' of 0 and 90° domain walls of length scale λ_c. More details on induced e_1, s_+, and s_- fields around the 'staircase' wall in Figs. 5b–d, their implication for functionality of the domain walls, and the displacement pattern are discussed in Ref. [6].

A similar approach is used to find elastic texture around structural defects. We consider impurity atoms at the centers of the square of four atoms, which couples to the e_1 mode distortion of the four nearest neighbor atoms. The corresponding energy expression is $E_{\text{sq,imp}} = E_{\text{sq,lat}} + E_{\text{imp}}$, where $E_{\text{sq,lat}}$ is Eq. (5) and E_{imp} is

$$E_{\text{imp}} = \sum_{\vec{i}} C_1 e_1(\vec{i}) h_1(\vec{i}). \tag{7}$$

Here, $h_1(\vec{i})$ is 1 if there is a defect at the site at $\vec{i} + (1/2, 1/2)$, and zero otherwise. C_1 represents the strength of the coupling. $E_{\text{sq,imp}}$ is minimized about e_1, e_2, e_3, s_+, and s_- with constraints among them for given h_1, which gives the relations between the relaxed strain fields and the h_1 field. Explicit expressions of these relations will be presented elsewhere. As a simple case, we show the elastic texture around a *single* defect in Figs. 4c and d.

To illustrate the influence of lattice deformation on electronic properties, we couple the twin boundary and defect solutions obtained above with the electronic degree of freedoms in a model of superconductors. The electronic model Hamiltonian is defined on a square lattice:

$$\mathcal{H} = -\sum_{ij,\sigma} \tilde{t}_{ij} c_{i\sigma}^{\dagger} c_{j\sigma} \sum_{i,\sigma} (\epsilon_i - \mu) c_{i\sigma}^{\dagger} c_{i\sigma} + \sum_{ij} (\Delta_{ij} c_{i\uparrow}^{\dagger} c_{j\downarrow}^{\dagger} + \Delta_{ij}^{*} c_{j\downarrow} c_{i\uparrow}). \tag{8}$$

Here $c_{i\sigma}$ annihilates an electron of spin σ on site i. The quantities ϵ_i and μ are the on-site impurity potential (if any) and the chemical potential, respectively. The hopping integral $\tilde{t}_{ij}$ is modified by the lattice distortion. The electron–lattice coupling is approximated by $t_{ij} = t_{ij}^0[1 - \alpha\epsilon_{ij}]$, where t_{ij}^0 is the bare hopping integral, ϵ_{ij} is the lattice-distortion variable, and α is the coupling constant. In our nearest neighbor realization, the bare hopping integral t_{ij}^0 is t for nearest neighbor sites and zero otherwise.

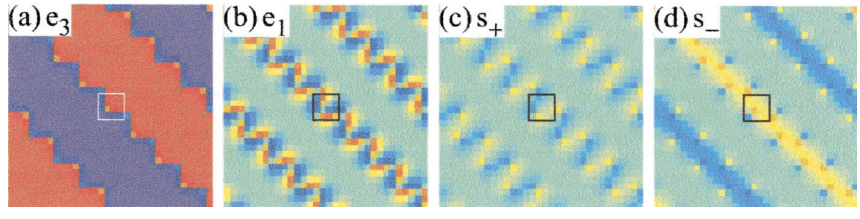

Fig. 5. Atomic scale domain wall solution for materials with $\lambda_c > 1$. Parameter values are $A_1 = 1$, $A_2 = 4$, $A_3' = 4$, $B = 5$, and $F_3 = 50$. Strain e_2 is zero.

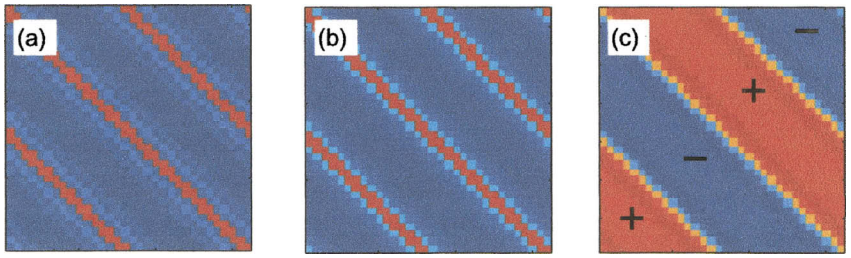

Fig. 6. Spatial variation of the SC OP for periodic twin boundaries displayed in Fig. 4a—(a) The s-wave OP in an s-wave superconductor and (b) the d-wave; and (c) extended s-wave components of the OP in a d-wave superconductor. The electron–lattice coupling constant $\alpha = 3$.

Specifically, we take the form of the lattice distortion to be $\epsilon_{ij} = [|(\mathbf{R}_j + d_j) - (\mathbf{R}_i + d_i)|/|\mathrm{R}_j - \mathbf{R}_i|]$, where $\{\mathbf{R}_i\}$ are the undistorted lattice coordinates and $\{\mathbf{d}_i\}$ the lattice displacement vectors with respect to $\{\mathbf{R}_i\}$. We assume an effective superconducting gap function given by $\Delta_{ij} = \frac{U_{ij}}{2}\langle c_{i\uparrow}c_{j\downarrow} - c_{i\downarrow}c_{j\uparrow}\rangle$, where $U_{ij} = U\delta_{ij}$ (i.e., attractive Hubbard-U model) for s-wave superconductivity and $U_{ij} = V\delta_{i+\gamma,j}$ (with γ specifying the nearest neighbors to the i-th site) for d-wave superconductivity. By performing a Bogoliubov–Valatin transformation, we may diagonalize Eq. (8) by solving the Bogoliubov–de Gennes (BdG) equation [7]:

$$\sum_j \begin{pmatrix} \mathcal{H}_{ij} & \Delta_{ij} \\ \Delta^*_{ij} & -\mathcal{H}^*_{ij} \end{pmatrix} \begin{pmatrix} u^n_j \\ v^n_j \end{pmatrix} = E_n \begin{pmatrix} u^n_i \\ v^n_i \end{pmatrix}, \qquad (9)$$

subject to the self-consistency conditions for the superconducting (SC) order parameter (OP):

$$\Delta_{ij} = \frac{U_{ij}}{4} \sum_n \left(u^n_i v^{n*}_j + v^{n*}_i u^n_j\right) \tanh\left(\frac{E_n}{2k_B T}\right). \qquad (10)$$

Here the single particle Hamiltonian reads $\mathcal{H}_{ij} = -\tilde{t}_{ij} + (\epsilon_i - \mu)\delta_{ij}$. We numerically solve the BdG equations self-consistently. Below, we report results for two types of local lattice distortions at zero temperature—a superlattice formed by twin boundaries and a single defect [8]. We measure the length and energy in units of a_0 (the undistorted lattice constant) and t. The chemical potential $\mu = 0$ and no extrinsic impurity scattering is introduced ($\epsilon_i = 0$). The pairing interaction for both the s-wave (U) and d-wave (V) superconductors is taken to be 3. The typical system size is $N_\mathrm{L} = 32 \times 32$ with periodic boundary conditions. When the local quasiparticle density of states (LDOS) is computed, we implement a much larger system using the above small system as a supercell.

In Fig. 6, we show the spatial variation of the SC OP induced by the deformation of Fig. 4a in both s- and d-wave superconductors. In both cases, the OP is lowered within the domain and is elevated at the domain wall (Fig. 6a,b). The magnitude of the OP is depressed in comparison to an undistorted square lattice since the lattice deformation changes the band structure, leading to a reduction in normal density of states at the Fermi energy. Even at the domain wall, where the strain-induced deformation is weakest, the amplitude of the enhanced OP is smaller than its value in an undistorted square lattice. This is due to the confinement from the two neighboring domains. In a twinned domain of a d-wave SC, a subdominant extended s-wave component is generated in a real combination d ± s. Because the symmetries of two twinned domains are reflected into each other with respect to the twin boundary, the relative phase between the d- and s-wave components switches by π when a twin boundary is crossed (Fig. 6c).

We show in Fig. 7 the spatial variation of the superconducting OP around the single defect (Fig. 4c) in both the s- and d-wave superconductor cases. The OP is depressed at the center of the defect, and reaches its defect-free bulk value at the scale of the superconducting coherence length. Notice that for a lattice-deformation defect, which affects the local electron hopping integral, the OP has a minimum at four sites surrounding the defect center. It is different from the case of an externally substituted unitary impurity, where the minimum OP is located only at the impurity site itself [9]. The range of influence of such a defect can be very large depending on the strength of electron–lattice coupling—*the elasticity propagates the electronic response*. The d-wave energy gap has a sign change at the nodal directions of the essentially cylindrical Fermi surface, but the d-wave OP does not exhibit such a sign change in real space. With

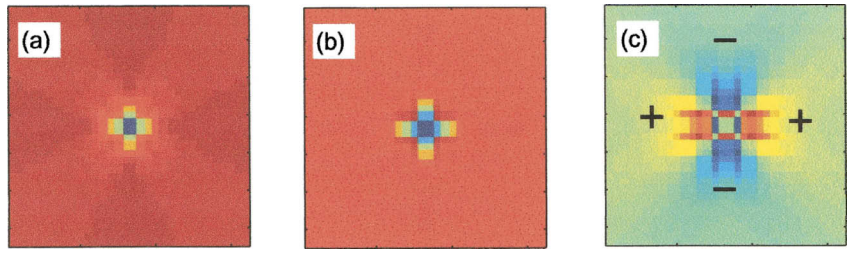

Fig. 7. Spatial variation of the SC OP for a single defect displayed in Fig. 4c—(a) The s-wave OP in an s-wave superconductor and (b) the d-wave; and (c) extended s-wave components of the OP in a d-wave superconductor. The electron–lattice coupling constant $\alpha = 3$.

the defect, an extended s-wave component of the OP is induced when the dominant d-wave component is depressed at the defect. Strikingly, the induced s-wave component has a sign change across the diagonals of the square lattice, i.e., sgn[cos(2θ)], where θ is the azimuthal angle with respect to the crystalline x axis. This is a direct manifestation of the d-wave pairing symmetry in real space.

Once the self-consistency for the order parameter is obtained, we calculate the LDOS:

$$\rho_i(E) = -\sum_n \left[\left|u_i^n\right|^2 f'(E - E_n) + \left|v_i^n\right|^2 f'(E + E_n) \right], \tag{11}$$

where $f'(E)$ is the derivative of the Fermi distribution function with respect to the energy. The LDOS determines the differential tunneling conductance, measurable by STM experiments [10]. Figure 8 shows the LDOS at a domain wall for both types of superconductors, where the modulation of the OP forms a superlattice, with maximum at the domain wall playing the role of an off-diagonal potential barrier (Δ_{ij} in Eq. (9)). For an s-wave superconductor, the quasiparticles are gapped away with their energy below the minimum SC OP. Outside the minimum of the pair potential, energy bands are formed by the quasiparticle scattering off the off-diagonal energy barriers at the domain walls. Interestingly, the bottom of the oscillation pattern follows the LDOS (gray line) of a system formed by a uniform rectangular domain. Similar oscillations are obtained for the d-wave superconductor. However, the bottom of the oscillations do not follow the single domain DOS (gray line). In addition, weak subgap peaks (labeled by arrows in Fig. 8b) appear symmetrically in the LDOS on the domain wall but are absent in the single-domain LDOS. We speculate that these resonant states are due to the gradient of the s-wave gap component induced inside the domain.

In Fig. 9, we show the calculated LDOS near the center of a single defect. The depression of the SC

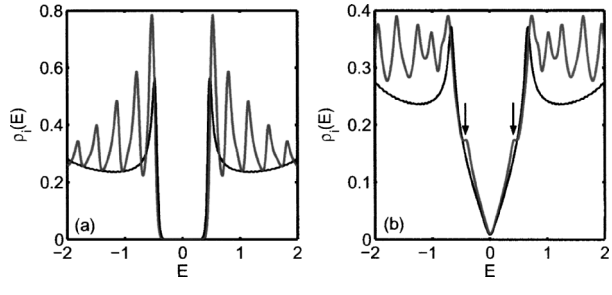

Fig. 8. The LDOS at a twin boundary in s-wave (a) and d-wave (b) superconductors. Also shown are the LDOS (gray lines) for a uniform domain. The electron–lattice coupling constant $\alpha = 3$.

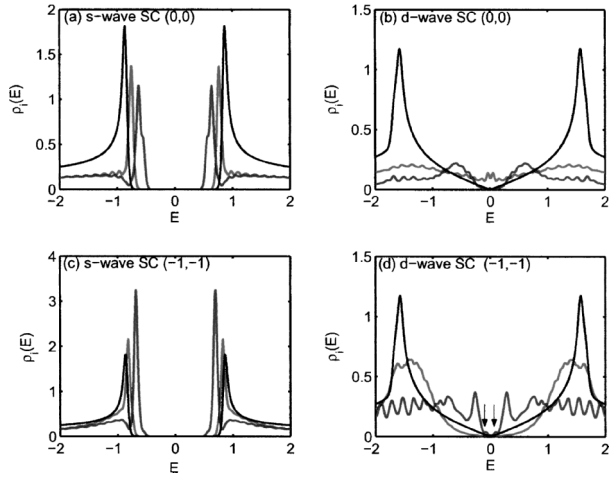

Fig. 9. (The LDOS near the center of a defect in s-wave (left column) and d-wave (right column) superconductors. The distance of the measured point away from the defect is labeled by its coordinate. The electron–lattice coupling constants are $\alpha = 3$ (dark gray lines) and 10 (black lines). Also shown is the defect-free LDOS (light gray lines).

OP at the defect makes a quantum-well-like profile of the energy gap. The size and depth of the well is determined by the electron–lattice coupling constant. In the s-wave superconductor, the well is shallow and small for weak coupling, which cannot trap low-lying quasiparticle bound states; for strong coupling constants, the well is deep and large so that subgap quasiparticle bound states are induced (the dark gray and black lines of Figs. 9a and c). The energy of these low-lying states must be in-between the bottom and edge of the well. Therefore, it is notable that the energy of these subgap states is shifted toward the Fermi surface as the electron–lattice coupling is increased (the black line in Fig. 9a and c). The electronic structure at the defect in a d-wave superconductor becomes even richer: For $\alpha = 3$ (weak coupling as compared to the band width of the uniform square lattice), the lattice distortion plays the role of a weak defect for the quasiparticle scattering. In this case, a resonant peak with a dip exactly at the Fermi energy is seen (the dark gray line in Fig. 9b). The overall peak comes from the scattering of quasiparticles off the single-particle off-diagonal potential (i.e., local change of the hopping integral as a response to the lattice deformation). This lattice-deformation-induced resonance state also exhibits Friedel oscillations. Typically, the peak structure appears in the LDOS at (0,0) (we label the four sites surrounding the defect center by (0,0), (1,0), (1,1), (0,1)) and $(-2,-2)$. For $\alpha = 10$ (strong coupling), the 'resonant' peaks are pushed to higher energies ($\simeq \pm 0.3$) (the black line of Fig. 9d). Furthermore, small shoulders appear close to the Fermi energy (the black lines of Figs. 9b and d), which are precursors of new Andreev resonance states. We have also computed the LDOS without imposing self-consistency on the OP and found that the double-peak structure is V-shaped with no existence of the shoulders. Therefore, the new Andreev resonance states originate from the confinement of the induced s-wave OP. All these features are unique to an elastic defect in a d-wave superconductor with short coherence length.

In summary, we have reported an approach to "atomic-scale elasticity," which uses symmetry modes of elementary objects of atoms as distortion variables. A gradient expansion for the energy with *anisotropic* coefficients has been obtained, with corrections to the phenomenological isotropic gradient terms often used in LG theory. As an illustration, we obtained domain wall (twin boundary) solutions and elastic texture around a defect in terms of strain *and* intracell modes, and showed how the domain wall solutions differ from the continuum elastic soliton solution [4]. Using these atomic scale profiles of elastic texture, we studied the influence of elastic lattice deformation on the nanoscale electronic structure in superconductors within a BdG approach. We showed that the SC OP is depressed in the regions where the lattice deformation exists. The calculated LDOS suggests that the electronic structure is strongly modulated in response to the lattice deformation. In particular, it is possible to trap low-lying quasiparticle states around the defects. Images of these states will make manifest the underlying long-range anisotropic elastic lattice deformation. These predictions can be directly tested by, e.g., STM experiments in new superconducting materials. Our approach is readily extended to other elastic textures, SC symmetries, and lattices, as well as coupling to other electronic models (for charge-transfer, charge-density-wave, spin-density-wave, Jahn–Teller, double-exchange, etc.).

ACKNOWLEDGMENTS

We thank A. J. Millis and S. R. Shenoy for insightful discussions. This work was supported by the U.S. Department of Energy.

REFERENCES

1. For a review, see Y. Bar-yam, T. Egami, J. Mustre-de Leon, and A. R. Bishop, eds., *Lattice Effects in High-T_c Superconductors* (World Scientific, Singapore, 1992); E. Dagotto, ed., *Nanoscale Phase Separation and Colossal Magnetoresistence* (Springer, New York, 2003); A. R. Bishop, S. R. Shenoy, and S. Sridhar, eds., *Instrinsic Multiscale Structure and Dynamics in Complex Electronic Oxides* (World Scientific, Singapore, 2003).
2. S. Stemmer, S. K. Streiffer, F. Ernst, and M. Ruhle, *Phil. Magn. A* **71,** 713 (1995).
3. S. R. Shenoy, T. Lookman, A. Saxena, and A. R. Bishop, *Phys. Rev. B* **60**(R12), 537 (1999); T. Lookman, S. R. Shenoy, K. Rasmussen, A. Saxena, and A. R. Bishop, *Phys. Rev. B* **67,** 024114 (2003).
4. G. R. Barsch and J. A. Krumhansl, *Phys. Rev. Lett.* **53,** 1069 (1984).
5. For example, $e_3(i) = [-d^x(i) + d^y(i) + d^x(i + (10)) + d^y(i + (10)) + d^x(i + (11)) - d^y(i + (11)) - d^x(i + (01)) - d^y(i + (01))]/2\sqrt{2}$.
6. K. H. Ahn, T. Lookman, A. Saxena, and A. R. Bishop, *Phys. Rev. B* **68,** 92101 (2003).
7. P. G. de Gennes, *Superconductivity of Metals and Alloys* (Addison-Wesley, New York, 1989).
8. For more details, see J.-X. Zhu, K. H. Ahn, Z. Nussinov, T. Lookman, A. V. Balatsky, and A. R. Bishop, *Phys. Rev. Lett.* **91,** 57004 (2003).
9. J.-X. Zhu, T. K. Lee, C. S. Ting, and C.-R. Hu, *Phys. Rev. B* **61,** 8667 (2000).
10. S. H. Pan, E. W. Hudson, K. M. Lang, H. Eisaki, S. Uchida, and J. C. Davis, *Nature* **403,** 746 (2000).